IOPscience iopscience.iop.org

Home Search Collections Journals About Contact us My IOPscience

Simulation of the lattice statics and dynamics of the perovskites $KMnF_3$ and $KZnF_3$

This article has been downloaded from IOPscience. Please scroll down to see the full text article.

1989 J. Phys.: Condens. Matter 1 7801

(http://iopscience.iop.org/0953-8984/1/42/003)

View the table of contents for this issue, or go to the journal homepage for more

Download details:
IP Address: 171.66.16.96
The article was downloaded on 10/05/2010 at 20:36

Please note that terms and conditions apply.

J. Phys.: Condens. Matter 1 (1989) 7801–7817. Printed in the UK

Simulation of the lattice statics and dynamics of the perovskites $KMnF_3$ and $KZnF_3$

R R Becher†, M J L Sangster‡ and D Strauch†

† Institut für Theoretische Physik, Universität Regensburg, D-8400 Regensburg, Federal Republic of Germany

‡ J J Thomson Physical Laboratory, University of Reading, Reading RG6 2AF, UK

Received 31 March 1989

Abstract. Interionic potentials for the cubic perovskite crystals $KMnF_3$ and $KZnF_3$ are derived and used in calculations of the configurational energies of intrinsic and substitutional defects. The pressure dependences of soft-mode frequencies and elastic constants are investigated as well as the temperature dependence of the former. Structural, elastic and vibrational properties in the tetragonal phase are estimated. Some results are obtained which probe the effects of impurities on displacive phase transitions.

1. Introduction

Over the past few years considerable progress has been made in modelling the static and dynamic properties of impure crystals which can be considered as mixtures of members drawn from particular families of ionic crystals, such as alkali halides and transition metal oxides. These advances have been made possible by the development of reasonably realistic consistent potential models for the families and the parallel development of general purpose computer codes for solving problems in defect statics, such as relaxations around impurities and the calculation of the energies of these relaxed configurations, and, more recently, in defect dynamics where modes of vibration of impurity systems may now be routinely analysed.

In this paper we attempt to apply this approach to two cubic perovskites, $KMnF_3$ and $KZnF_3$. The main distinction of interest between these two crystals is that the former undergoes a displacive structural phase transition to a tetragonal form at 186 K whereas the latter remains cubic down to the lowest temperatures. The phase transition in $KMnF_3$ is generally believed to be second order although there is some experimental evidence (see, e.g., Shirane *et al* 1970) that it may be weakly first order. There have been several studies of these crystals, notably the investigation of defect statics in $KMnF_3$ by Kilner (1981) and the inelastic neutron scattering measurements on both crystals together with extensive analysis in terms of force constant models by Lehner *et al* (1982). Our development of potentials in the next section follows the work of Kilner fairly closely with the additional constraints imposed by the consistency which we require for consideration of the substituted systems $KMnF_3$:Zn and $KZnF_3$:Mn. Similar constraints are imposed in some of the lattice dynamical models investigated by Lehner *et al* but, since these employ force constants rather than being derived from potential models, a unified approach to both defect statics and defect dynamics is not possible.

0953-8984/89/427801+17$02.50 © 1989 IOP Publishing Ltd

In §3 we present the results of some room-temperature defect energy calculations for both crystals based on the potentials obtained in §2. We have recalculated the cases considered earlier by Kilner (1981) for $KMnF_3$ and find that in most cases there is little change of significance between the results produced from our potential and those from his. Parallel calculations for $KZnF_3$ are also presented together with some results for the substitution of Zn in $KMnF_3$ and Mn in $KZnF_3$. Volumes of substitution are obtained and interpreted in terms of departures from Vegard's rule along the lines of a similar study of mixed alkali halides by Cox and Sangster (1985).

In §4 we consider the dynamics of the pure crystals, in particular the dependence of the soft-mode frequencies on temperature and pressure. Our models show qualitatively the main distinction between the two crystals, the onset of mode instability for $KMnF_3$ but not for $KZnF_3$. Calculations of structural, elastic and vibrational properties of $KMnF_3$ in its tetragonal phase are presented in the following section. In §6 we investigate possible roles of impurities in either quenching the phase transition in $KMnF_3$ or promoting it in $KZnF_3$. We tentatively conclude that the presence of low concentrations of Mn impurities in $KZnF_3$ does not result in the crystal having a non-cubic phase but that Zn impurities at concentrations up to 10% in $KMnF_3$ lower the pressure at which a transition to the tetragonal phase is induced.

2. Interatomic potentials for $KMnF_3$ and $KZnF_3$

In order to reduce the number of free parameters in potential models for these fluoride perovskites it is normal to transfer potentials for the K–F and F–F short-range interactions from models for alkali halides. (The K–K interaction might also be taken from these sources but, in view of the large separation of K ions in the perovskite structure, these interactions are generally ignored.) Similarly the shell model polarisation parameters, that is, shell charges and isotropic shell–core force constants, for the K and F ions found in work on the alkali fluorides may be used in the perovskites. To complete the description, parameters for some assumed form for the X–F (X = Mn or Zn) interaction and the polarisation parameters for X are required: again X–X short-range interactions can be ignored on the grounds of the large distances between these ions. Values for these relatively few parameters may be found by imposing stability constraints and fitting to available experimental data such as a selection from elastic constants, dielectric constants and phonon dispersion relations. Essentially this is the approach adopted by Kilner (1981) for $KMnF_3$ and by Lehner *et al* (1982) for both $KMnF_3$ and $KZnF_3$. It will also be adopted here. Comparisons with these other potential models will be made.

There is a considerable choice of alkali and alkaline earth halide models from which to select the K–F and F–F terms. To keep open the possibility of modelling mixed systems it is necessary to have a single description of interactions which are common to the two pure crystals. Initially the model of Sangster and Atwood (1978) was tried for K–F and F–F interactions together with their polarisabilities for F and K ions, α_F and α_K. The shell charges Y_F and Y_K were left as free parameters, the shell–core force constants being determined by the relations

$$\alpha_i = \frac{Y_i^2}{k_i/V} \tag{1}$$

which define the free-ion polarisabilities. V is the volume of the unit cell, and the force constants k_i are scaled dimensionless quantities, the unscaled constants being $(e^2/V)\,k_i$

in the usual way. The ionic charges of K and F ions, Z_K and Z_F, were also free parameters but taken to be the same in both $KMnF_3$ and $KZnF_3$. The common ionic charge for Mn and Zn (Z_X) is given by charge neutrality. Thus four free parameters are used in the description of common interactions. Additionally each crystal has four further parameters, two for the interaction between X and F, which is assumed to have the simple Born–Mayer form

$$\phi_{X-F}(r) = B \exp(-r/\rho) \tag{2}$$

and two for the polarisation parameters α_X and Y_X.

We may remove two of these twelve parameters for modelling the pair of crystals by imposing the equilibrium conditions

$$\left(\frac{1}{r}\frac{d\phi_{X-F}}{dr}\right)_{r=r_0} + 4\left(\frac{1}{r}\frac{d\phi_{K-F}}{dr} + \frac{1}{r}\frac{d\phi_{F-F}}{dr}\right)_{r=\sqrt{2}r_0} = -\frac{2}{3}\frac{e^2}{V}\alpha_M \tag{3}$$

where r_0 is the equilibrium nearest-neighbour X–F distance, i.e. half the lattice constant (a_0), and α_M is the Madelung constant defined so that the electrostatic energy per unit cell is $e^2\alpha_M/a_0$. Cowley (1964) gives the following expression for the Madelung constant:

$$\begin{aligned}\alpha_M = {} & 1.259\,50\,(Z_K^2 + Z_X^2) + 4.571\,09\,Z_F^2 + 0.79\,260\,Z_K Z_F \\ & - 0.667\,17\,Z_X Z_F + 0.483\,62\,Z_K Z_X\end{aligned} \tag{4}$$

(although he states, incorrectly, that the electrostatic energy per unit cell is then $2e^2\alpha_M/a_0$).

The remaining parameters were then adjusted to give a best fit to the dispersion curves obtained from neutron scattering experiments by Lehner *et al* (1982). Apart from the reduction in the number of free parameters, the essential differences between our model and the model SM1 of Lehner *et al* are that we use only central potentials satisfying the equilibrium condition and that we insist on a unique description of the elements common to the two crystals. Although our fit to the dispersion for $KZnF_3$ was quite satisfactory, the results for $KMnF_3$ were extremely bad.

Dispersion curves produced by models are particularly sensitive to the choice of F–F interaction despite the fact that the force constants from this interaction are small compared with those from the X–F interaction. Most model F–F potentials have a minimum close to the separation between fluorine ions in the perovskites (2.96 Å in $KMnF_3$, 2.87 Å in $KZnF_3$). The minimum in the spline potential of Catlow *et al* (1977b) is placed at 2.726 Å, that of Catlow *et al* (1977a) at 2.833 Å. One of our interests in this paper will be in studying the behaviour of low-frequency modes when pressures are imposed on the crystals. It is clear that the F–F force constants will depend very sensitively on pressure.

We found that using the Buckingham potential of Sangster and Atwood (1978)

$$\phi(r) = A\exp(-r/\rho) - \frac{C}{r^6} - \frac{D}{r^8} \tag{5}$$

instead of the K–F Born–Mayer potential and that replacing the F–F potential by the spline potential of Catlow *et al* (1977b),

$$\phi(r) = \begin{cases} A\exp(-r/\rho) & r < r_b \\ \text{fifth-order polynomial} & r_b < r < r_m \\ \text{third-order polynomial} & r_m < r < r_a \\ -C/r^6 & r_a < r \end{cases} \tag{6}$$

while retaining the other potentials and polarisabilities as above, resulted in greatly improved fits to the dispersion relations. The parameters of our model, including those taken from other potentials as well as those fitted to dispersion curves, are given in table 1. The ten coefficients required to specify the two polynomials for the F–F interaction are determined by continuity at the knots of the potential and its first and second derivatives together with the siting of one knot at the minimum r_m. In figure 1 we show the phonon dispersion from our model together with measured frequencies from Lehner *et al* (1982).

Table 1. Model potential parameters for $KMnF_3$ and $KZnF_3$, satisfying equilibrium condition for lattice constants 4.19 Å and 4.054 Å respectively.

(*a*) Charges (in units of $|e|$) and polarisation force constants (in units of eV Å^{-2}), cf equation (1).

X	Z_X	Y_X	k_X
K	8.62	−7.655	797.579
F	1.639 33	−2.64	102.920
Mn	8.167	−6.13	1964.670
Zn	3.429	−1.392	608.644

(*b*) Buckingham potentials, cf equation (5).

	A (eV)	ρ (Å)	*C* (eV Å^6)	*D* (eV Å^8)
Mn–F	1654.780	0.275 91	0.0	0.0
Zn–F	1655.530	0.265 16	0.0	0.0
K–F	2693.740	0.284 40	29.18	26.49

(*c*) Spline potential for the short-range F–F interaction, cf equation (6).

A (eV)	ρ (Å)	*C* (eV Å^6)	r_b (Å)	r_m(Å)	r_a (Å)
1127.70	0.2753	15.83	2.000	2.726	3.031

The procedure adopted by Kilner (1981) in establishing his potentials for $KMnF_3$ was broadly similar. The equilibrium condition is not satisfied exactly as is evident from the elastic constants which Kilner derives from his potentials and which show a small departure from the Cauchy relation. We have calculated the dispersion relation in the [111] direction from Kilner's potential and find that near the R point the modes are unstable. After some modifications to the Mn–F potential to restore equilibrium, these mode instabilities are removed.

Cowley (1964) gives expressions for the elastic constants in terms of force constants. (As in the definition of the Madelung constant, his expressions are only correct if his r is taken as the full lattice spacing a_0.) In table 2 we give the values obtained from our model with, for comparison, results from measurements by Aleksandrov *et al* (1966) for $KMnF_3$ and by Gesland *et al* (1972) for $KZnF_3$. The model values have to satisfy the Cauchy relation, $C_{12} = C_{44}$. The values found are in reasonable agreement with the average $\frac{1}{2}(C_{12} + C_{44})$, and also the calculated constants C_{11} are close to those determined experimentally. Of course, since our fits to dispersion relations have included acoustic branches, a fair level of agreement with elastic constants is ensured.

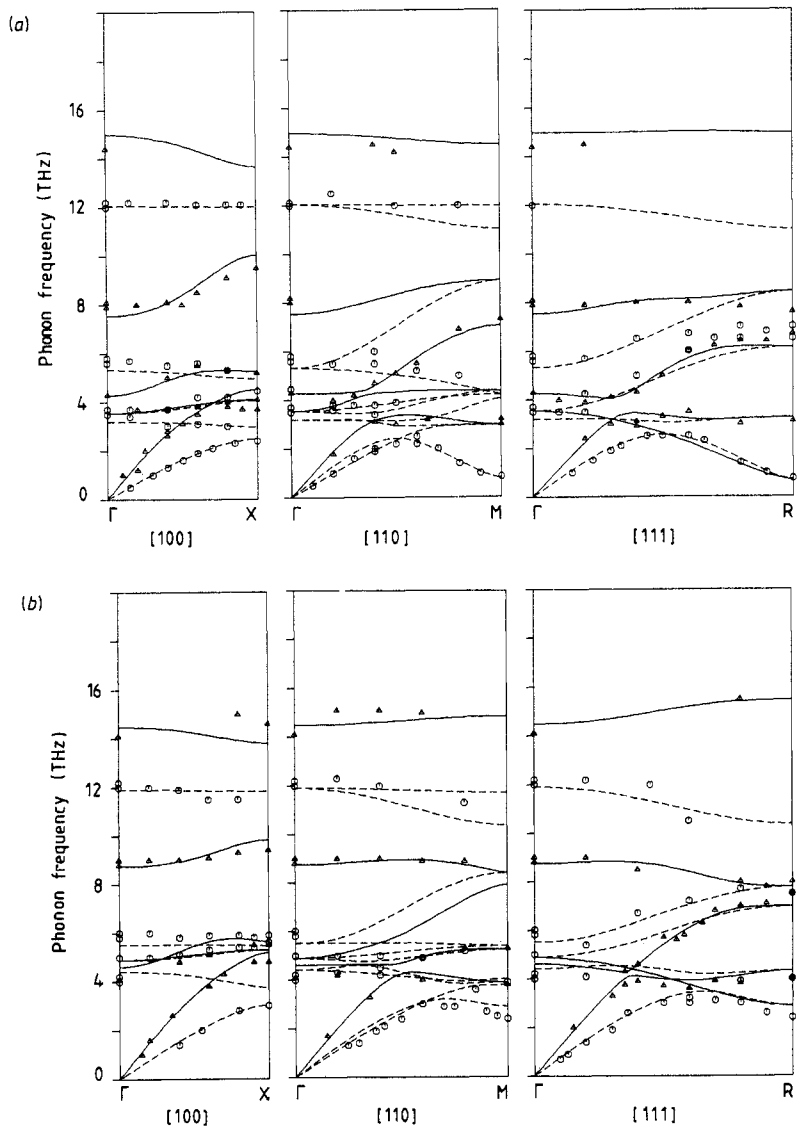

Figure 1. Dispersion relations for (*a*) $KMnF_3$ and (*b*) $KZnF_3$. Full (broken) curves are theoretical longitudinal (transverse) phonon branches. Triangles and circles are measured longitudinal and transverse phonons from Lehner *et al* (1982), Gesi *et al* (1972) and Rousseau *et al* (1981).

The table also gives the static and high-frequency dielectric constants evaluated from the potential models by the standard procedures detailed by Cowley (1962); in fact we used the PLUTO code (Norgett 1974), which follows the procedures in our calculations. Measured constants from Perry and Young (1967) are quoted for comparison; the alternative higher measured ε_0 for $KMnF_3$ is from Gesi and Ozawa (1973).

By repeating the calculations of the elastic constants at different lattice parameters, estimates of dC_{ij}/da can be obtained and, hence, using the model isothermal

Table 2. Perfect lattice properties obtained experimentally and from the model potential.

	Elastic constants				Dielectric constants		
	C_{11} (GPa)	C_{12} (GPa)	C_{44} (GPa)	Ref.	ε_0	ε_∞	Ref.
$KMnF_3$							
Experiment	115.0	39.5	27.4	a	9.02	2.10	c
					9.72		d
Model	142.7	31.2	31.2		10.77	1.94	
$KZnF_3$							
Experiment	134.5	52.7	38.1	b	7.78	2.34	c
Model	160.7	43.9	43.9		8.14	1.98	

[a] Aleksandrov *et al* (1966).
[b] Gesland *et al* (1972).
[c] Perry and Young (1967).
[d] Gesi and Ozawa (1973).

compressibility,

$$K_T = 3(C_{11} + 2C_{12})^{-1} \tag{7}$$

values for the pressure derivatives of the elastic constants. In table 3 values at room temperature for $KMnF_3$ are given together with recent experimental results by Cao and Barsch (1988). Large parts of the discrepancies arise from differences between theory and experiment for the elastic constants themselves.

Table 3. Pressure derivatives of isothermal elastic constants for $KMnF_3$ at room temperature.

	dC_{11}/dP	dC_{12}/dP	dC_{44}/dP
Model	9.77	1.59	1.07
Experiment[a]	5.82	3.29	0.28

[a] Cao and Barsch (1988).

3. Calculations of defect energies

We have used our model potential in calculations of the energies of a variety of defect configurations in $KMnF_3$ and $KZnF_3$. The calculations were performed using the HADES code (Norgett 1974, 1977). We have obtained results for all the intrinsic defect configurations considered by Kilner (1981). Since both the defect geometries and computational details are fully described in Kilner's paper, it will suffice to present our results in a form which closely follows that used by Kilner; this is done in table 4. For $KMnF_3$ we list in parentheses the corresponding results from Kilner's work. $KZnF_3$ was not considered by him.

The agreement between our calculations and those of Kilner for $KMnF_3$ is fairly close. In all cases our formation energies are lower than Kilner's, and this is most

Table 4. Intrinsic defect energies (eV) for $KMnF_3$ and $KZnF_3$. Values in brackets are from Kilner (1981).

	$KMnF_3$		$KZnF_3$
(*a*) Formation energies for single defects			
Mn/Zn vacancy	23.29		24.47
K vacancy	5.30		5.53
F vacancy	5.67		6.07
Mn/Zn interstitial	−16.40		−17.06
K interstitial	−1.58		−0.69
F interstitial	−2.72		−1.84
F interstitialcy	−2.98		−2.18
(Cohesive energy/cell	−37.91	(−36.47)	−39.39)
(*b*) Formation energy of neutral defects			
Anion Frenkel			
(i) vacancy + interstitial	2.95	(2.91)	4.23
(ii) vacancy + interstitialcy	2.69	(2.79)	3.89
K Frenkel	3.72	(3.92)	4.84
Mn/Zn Frenkel	6.89	(8.36)	7.41
Schottky quintet	7.69	(7.91)	8.82
(*c*) Activation energies			
K vacancy	1.57	(1.63)	2.04
F vacancy	0.42	(0.41)	0.54
F interstitial	0.26	(0.12)	0.34

marked for the cation Frenkel defect formation energies. In agreement with Kilner, we find that a (100) dumbell fluorine interstitialcy is more stable than an isolated fluorine interstitial, in our calculations by 0.27 eV. The most favourable transport process is fluorine interstitial migration by the interstitialcy mechanism taking the saddle point as the isolated interstitial configuration as in figure 2.

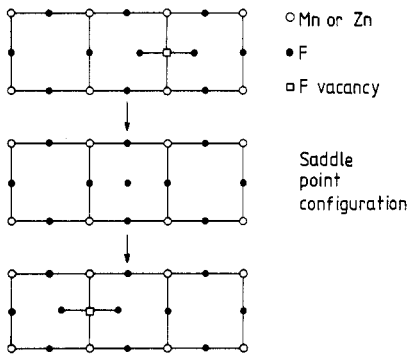

Figure 2. Fluorine interstitial migration by an interstitialcy mechanism.

Our conclusions on intrinsic defect formation and activation energies in $KZnF_3$ are very similar to those for $KMnF_3$. All energies are slightly higher in this case, that for anion Frenkel defect formation being perhaps the most significant.

We have also calculated the energies for the substitutions $KMnF_3$:Zn and $KZnF_3$:Mn. For these calculations it is essential that the potential models for the two host crystals use the same specifications for all common interactions, a feature which has been incorporated in our potentials. By investigating the dependence of these formation energies on lattice parameter, a, the volume of formation may be estimated by using the result discussed by Gillan (1981),

$$\Omega_f = \frac{1}{3} K_T \left(a \frac{\partial E_f}{\partial a} \right)_{a=a_0} \tag{8}$$

where K_T is the isothermal compressibility of the host crystal given by equation (7). For consistency it is important to use elastic constants calculated from the model rather than experimental values. If, for both substitutions, Ω_f is equal to ΔV, the difference in unit cell volumes for $KMnF_3$ and $KZnF_3$ (with the appropriate sign in each case), then the binary system $KMn_xZn_{1-x}F_3$ should satisfy Vegard's rule (Vegard 1921) in the form that states that the volume per formula unit scales linearly with concentration x.

Table 5. Energies and volumes of substitution in $KMnF_3$ and $KZnF_3$.

	$KMnF_3$:Zn	$KZnF_3$:Mn
E_f (eV)	−1.467	+1.494
Ω_f (Å^3)	−7.502	+6.879
ΔV (Å^3)	−6.933	+6.933

Our calculations of energies and volumes of substitution are given in table 5 together with ΔV. It can be seen that only minor departures from the predictions of Vegard's rule are found. Since the volumes of formation set the extremal slopes of a plot of volume against concentration, our results indicate that such a plot would lie below the Vegard straight line. In a similar analysis of mixed alkali halides, Cox and Sangster (1985) found the opposite behaviour. When x-ray scattering measurements of average spacings in mixed crystals are available they are generally plotted as deviations from an alternative version of Vegard's rule in which the linear spacing (rather than the volume) is taken to scale with concentration. In figure 3 we plot an estimate of these deviations over the complete composition range obtained by fitting the volume to a cubic polynomial in x with coefficients determined by the values and gradients at the end points. Since the maximum deviation of a_0 (4.054 and 4.190 Å at the end points) is less than 10^{-3} Å the limitations in accuracy of our calculations makes this conclusion somewhat tentative.

There have been measurements of the relaxations of fluorine ions around an Mn impurity in $KZnF_3$ by the following techniques: EXAFS (Leblé 1982), EPR (Barriuso and Moreno 1984) and interpretations of crystal-field splittings of spectral lines of the impurity (Rodríguez and Moreno 1986). The three techniques provide results which are consistent within the quoted accuracies of the measurements. The EXAFS determination of Leblé (as quoted by Barriuso and Moreno) is the least uncertain, giving the Mn–F distance as (2.08 ± 0.01) Å which is (2.6 ± 0.5) % greater than the host Zn–F distance. Our calculations give the outward relaxation as 2.82 %, in excellent agreement with the measurements.

Rodríguez and Moreno (1984) have also studied how the ratio r_0'/r_0 varies with temperature (r_0' is the Mn–F distance; r_0 the Zn–F distance) and found that it increases

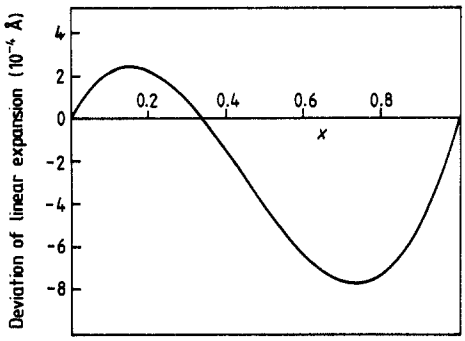

Figure 3. Deviation of calculated average lattice parameter for $KMn_xZn_{1-x}F_3$ from the value given by Vegard's lattice parameter rule.

with increasing temperature. In other words, as the lattice is expanded, the Mn–F distance increases at a faster rate than the host lattice parameter: in fact by more than twice the rate. By repeating our calculations with increased host lattice parameters we find the same trend but on a greatly reduced scale. Using the experimental lattice expansion coefficient, 1.5×10^{-5} K^{-1} for linear expansion, quoted by Ridou *et al* (1984) we estimate from our calculations that $(d/dT)(r_0'/r_0)$ is around 1.4×10^{-6} K^{-1} whereas from Rodríguez and Moreno's results we deduce $(23 \pm 15) \times 10^{-6}$ K^{-1}. Although the differencing involved in obtaining our estimate implies considerable uncertainty, it seems that our model potentials cannot produce an effect on anything like the scale suggested by the experimental measurements. While this is no doubt due in part to inadequacies of our model, it may be that some of the assumptions made in extracting experimental relaxations from the raw data, for example the assumption that certain crystal field parameters are independent of temperature, need further questioning.

4. Dynamics of cubic $KMnF_3$ and $KZnF_3$

The dispersion relations for the pure crystals obtained from our potential models have already been shown as figure 1. In this section we concentrate on the dynamical feature of particular interest in these perovskites, namely the mode softening at critical points as the temperature is reduced and any consequent phase transitions.

The dispersion branches to be studied are the lowest-frequency branches in the [111] and [110] directions, in particular the modes at the R_{25} and M_{15} points on the zone boundary in these directions. Measurements of the temperature dependence of the R_{25}-mode frequency in $KMnF_3$ have been made by Gesi *et al* (1972) and, more recently, in $KZnF_3$ by Lehner *et al* (1982), who also consider the M_{15} mode. To within experimental error the squared frequencies fall linearly with decreasing temperature in accord with the Landau theory for phase transitions. For $KMnF_3$ the R_{25} mode becomes unstable near the temperature of the transition from a cubic to a tetragonal phase at 186 K. In $KZnF_3$ the mode remains stable down to the lowest temperature, and the crystal does not undergo a phase transition. In both cases the M_{15} mode also softens as the temperature is reduced but this is insufficient for a phase transition to result. The dependence of the R_{25}-mode frequency on pressure has been reported by Ridou *et al* (1984).

The displacements in the soft R_{25} and M_{15} modes consist in both of cases of rotations of the F^- octahedra surrounding the divalent ions around one of their fourfold axes. From the crystal structure the rotations of adjacent octahedra in the plane with the chosen fourfold axis as normal must have opposing signs. For adjacent octahedra along the axis the rotations have the same sign in the M_{15} mode and the opposite sign in the R_{25} mode.

In figure 4 we show results of calculations with our potentials of the temperature and pressure dependences of the R_{25}-mode frequencies in the two pure crystals. For $KMnF_3$ the pressure dependence of the M_{15}-mode frequency is also shown. The temperature dependence is at atmospheric pressure and the pressure dependence at room temperature. We obtain first the variation in $v^2(a)$ with lattice parameter a within the quasi-harmonic approximation, that is, the same potential models are used but harmonic force constants are found from derivatives evaluated at changed atomic separations. When combined with the compressibilities of the crystals, this variation gives directly the pressure dependence of the mode frequencies at constant temperature. As discussed in the previous section in connection with volumes of formation, we use isothermal compressibilities calculated from the model potentials, taking account of the small variations in compressibility with changes in lattice parameter. These results are shown in figure 4(*a*) and 4(*b*).

For $KMnF_3$ there are no experimental results for comparison. Our model predicts that under pressure both the R_{25} and M_{15} modes soften with the former becoming unstable at around 16 kbar (at room temperature). For $KZnF_3$ experimental results are available over a rather restricted range (Ridou *et al* 1984) and are shown in figure 4(*b*) as a broken line. In this case the R_{25}-mode frequency given by our model is too high: there is some qualitative agreement between the theoretical and experimental pressure gradients but the model slope is too small by a factor of around 2.5. We believe that this error in the slope arises mainly as a consequence of the model frequency of the R_{25} mode at zero pressure being too high. If this frequency is brought down to the experimental value by suitable arbitrary adjustments to the potentials, the pressure gradient is found to be in good agreement with the experimental data.

We now consider the temperature dependence of the R_{25} and M_{15} modes. If we assume that mode frequencies vary with temperature only via the temperature dependence of the lattice constant (i.e. we make the quasi-harmonic approximation) then estimates of $v^2(T)$ can be obtained by combining the above calculations of $v^2(a)$ with coefficients of linear thermal expansion. We have calculated these coefficients by minimising the free energy

$$G(r, T) = \phi_0(r) + \sum_{qj} \left[kT \ln \left(2 \sinh \frac{\hbar\omega_{qj}(r)}{2kT} \right) - kT_0 \ln \left(2 \sinh \frac{\hbar\omega_{qj}(r)}{2kT_0} \right) \right] \tag{9}$$

where the adjustment to the usual expression is required since our potentials are fitted at a reference temperature T_0 (300 K). The results of our calculations of the linear expansion coefficient at 300 K with a sample of 1000 points in the (full) Brillouin zone are given in table 6 together with experimental determinations by Dormann *et al* (1977) for $KMnF_3$ and by Julliard (1974) (quoted by Ridou *et al* (1984)) for $KZnF_3$. For both crystals our calculations give values which are only slightly greater than the measurements. The temperature dependences of the soft modes calculated in this way are shown as dotted lines in parts (*c*) ($KMnF_3$) and (*d*) ($KZnF_3$) of figure 4. The experimental results of Gesi *et al* (1972) for $KMnF_3$ and Lehner *et al* (1982) for $KZnF_3$ are shown for comparison.

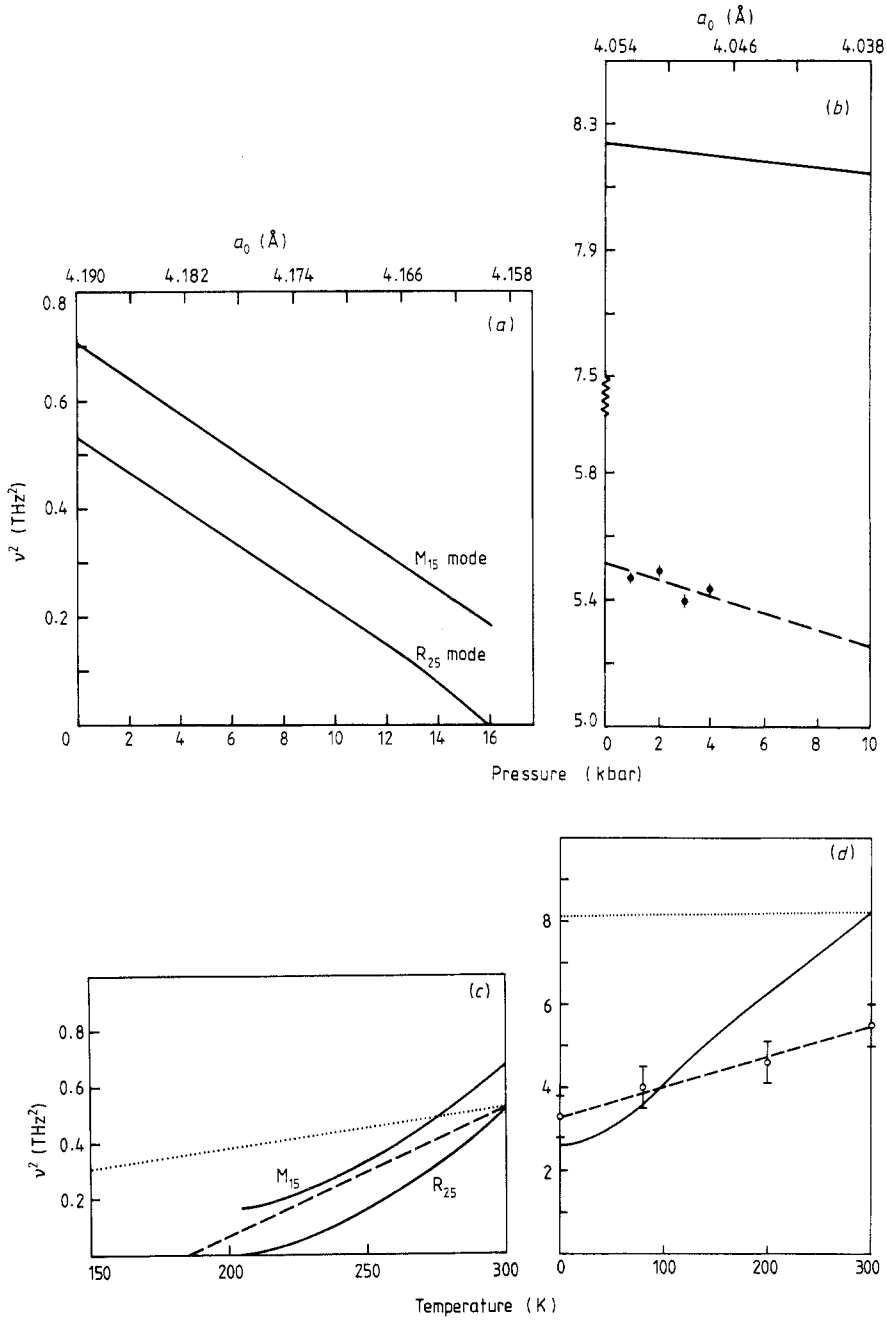

Figure 4. Pressure and temperature dependences of squares of soft mode frequencies in $KMnF_3$ (parts (*a*) and (*c*)) and $KZnF_3$ (parts (*b*) and (*d*)). Experimental results are shown as broken lines and are from Ridou *et al* (1984) in (*b*), Gesi *et al* (1972) in (*c*) and Lehner *et al* (1982) in (*d*). Dotted lines in (*c*) and (*d*) show the effect of just the thermal expansion.

That the agreement between these calculations and experiment is poor is not surprising. The investigations of soft modes in oxide perovskites ($SrTiO_3$ and $LaAlO_3$) by Feder and Pytte (1970) and also by Bruce and Cowley (1973), using parametrised

Table 6. Coefficients of linear thermal expansion at 300 K for $KMnF_3$ and $KZnF_3$ in units of 10^{-5} K^{-1}.

	Experiment	Model without anharmonicity	Model with quartic anharmonicity
$KMnF_3$	1.65[a]	1.98	0.72
$KZnF_3$	1.50±0.07[b]	1.58	1.26

[a] Dormann *et al* (1977).
[b] Julliard (1974).

models, showed that for an adequate description of mode softening it is essential to include the effects of third- and fourth-order anharmonicity in the potential. Leibfried and Ludwig (1961) have indicated that higher-order terms may be neglected. Here we shall restrict our investigations to the fourth-order anharmonic contributions. Apart from being simpler to calculate, they should provide the dominant correction. The calculations of Bruce and Cowley (1973) for $SrTiO_3$ indicated that corrections from the third-order anharmonicity were about half of those from fourth order and of the opposite sign.

The fourth-order anharmonic correction is calculated from the fourth derivative of the potentials of interaction between ions. We assume that it is sufficient to consider only the short-range part and, in our models, this acts only between shells. Then, in lowest order of the anharmonicity (similar to first-order perturbation theory), the anharmonic contribution $\delta\phi_{ij}$ to the force constants ϕ_{ij} acting between two atoms i and j is given by (see, for example, Cochran and Cowley 1967, Bruce and Cowley 1973, Bilz *et al* 1984)

$$\delta\phi_{ij} = \tfrac{1}{2}\phi_{ij}^{(4)}\left(\langle(s_i - s_j)^2\rangle_T - \langle(s_i - s_j)^2\rangle_{T_0}\right). \tag{10}$$

Here $\phi_{ij}^{(4)}$ is the fourth-order potential expansion coefficient, and s_i is the shell displacement of atom i; the second term in equation (10) is a correction as in equation (9). The approximation made in this expression for the contribution to the self-energy is equivalent to approximating

$$(4!)^{-1}(s_i - s_j)^4 \simeq \tfrac{1}{2}\langle(s_i - s_j)^2\rangle_T \, \tfrac{1}{2}(s_i - s_j)^2$$

in the fourth-order potential term.

Apart from the temperature dependence of the phonon frequencies through the effect of thermal expansion there is now a temperature dependence via the displacement fluctuations of equation (10). In equation (9) one has thus to make the replacement

$$\omega_{qj}(r) \to \omega_{qj}(r, T). \tag{11}$$

We have carried out self-consistent calculations for fixed r and T using equation (10) to correct the phonon frequencies. In practice, we have followed an iterative procedure using 8000 $\boldsymbol{q}$-vectors in the full Brillouin zone.

The entire operation is then repeated for different lattice spacings, but keeping the temperature fixed, until a minimum in the free energy is found. This then yields the anharmonic phonon frequencies and the lattice parameter at the given temperature. Our results for the M_{15} mode in $KMnF_3$ and the R_{25} mode for both $KMnF_3$ and

$KZnF_3$ are shown as full curves in figures 4(*c*) and 4(*d*) and the corrected linear expansion coefficients at 300 K are given in the final column of table 6. The frequencies are now in much better agreement with experiment although, as anticipated, the fourth-order anharmonicity over corrects. If, as Bruce and Cowley (1973) found for $SrTiO_3$, the third-order anharmonicity leads to changes in frequency of the opposite sign and about half the magnitude, excellent agreement with experiment would result. This is currently being investigated. In the calculations of the linear expansion coefficients, the addition of quartic anharmonicity again over-corrects the result found when anharmonicity is ignored. Here too it is to be expected that when cubic anharmonicity is included theory and experiment will be in better accord.

5. Properties of $KMnF_3$ the tetragonal phase

In this section we present some model predictions of the structural, elastic and vibrational behaviour of $KMnF_3$ after it has undergone the phase transition, which we achieve by lowering the lattice parameter. The results are collected in the three parts of figure 5.

5.1. Structural properties

As mentioned in the last section the phase transition is caused by a rotation of the F^- octahedron surrounding an Mn^{2+} ion. There is an accompanying tetragonal distortion with the lattice parameter along the axis of the F^- rotation (the *c* axis) becoming larger than that for the other axes. In the three parts of figure 5 results are plotted against a parameter $\bar{a}$, which is the cube root of the volume per formula unit and therefore passes continuously into the single lattice parameter for the cubic phase. In the tetragonal phase the primitive unit cell contains two formula units.

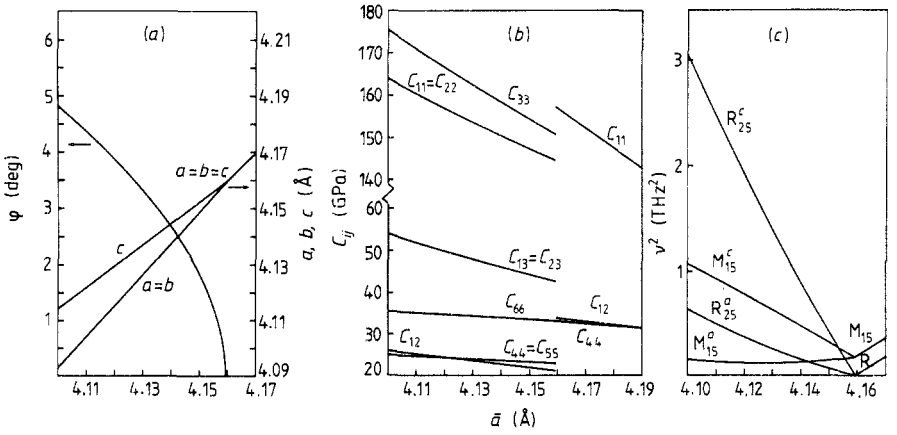

Figure 5. Properties of $KMnF_3$ as functions of $\bar{a}$ ($\bar{a}^3$ is the volume per formula unit): (*a*) angle of rotation of F^- octahedron and lattice parameters *a* and *c*/2; (*b*) elastic constants and (*c*) squared frequencies of soft modes.

We have developed a computer code which, from a given initial set of positions of the cores and shells of the ions, carries out relaxations of these positions (while keeping the volume of the cell constant) to find the equilibrium configuration of the cell at that fixed volume. This has been used to obtain the angle of rotation of the F^- octahedron and the lattice parameters c and a over a range of values of $\bar{a}$ as displayed in figure 5(*a*). The continuation of the lattice parameters into the cubic phase is indicated. The rotation angle varies continuously from zero at the phase transition, where it has a discontinuity in its first derivative characteristic of a second-order displacive phase transition. There are no experimental results with which these predictions can be directly compared although the measurements of the rotation angle as a function of temperature by Hirotsu and Sawada (1973) show a qualitatively similar behaviour near the transition.

5.2. Elastic constants

Calculations of the six elastic constants for crystals in equilibrium at a range of values of $\bar{a}$ are shown in figure 5(*b*), together with the cubic elastic constants from which they stem. (The slopes in the cubic phase provided the pressure derivatives given in table 3.) In the tetragonal phase there is again no experimental work for comparison. Note that on passing through the transition to the tetragonal phase the elastic constants are shifted (as well as being split) as may be expected in a second-order phase transition since the elastic constants involve second derivatives of the energy. The centroids of the pairs of elastic constants stemming from either C_{11} or C_{44} are shifted to lower values while the opposite is the case for the pair from C_{12}.

As has been seen in table 2 the model predictions of the room-temperature (cubic) elastic constants show some disagreement with experiment. Similar discrepancies are to be expected in the tetragonal phase results.

5.3. Soft modes

The squared frequency of the modes in the tetragonal phase which stem from the R_{25} and M_{15} modes in the cubic phase are shown as functions of $\bar{a}$ in figure 5(*c*). The cubic phase part of the diagram is, apart from a compressibility factor, as in figure 4(*a*). Each of the triply degenerate cubic phase modes gives rise to a doublet (superscript *a*) and a singlet (superscript *c*) in which the F^- vibrations are perpendicular to one of the *a* axes and to the *c* axis respectively.

Of particular interest is the M_{15}^a doublet which shows an initial decrease in v^2 as $\bar{a}$ is lowered from its value at the transition but then increases slowly after $\bar{a}$ has fallen below about 4.125 Å. This mode is believed to be responsible for a further phase transition at 78 K which Okazaki and Suemune (1961) and Shirane *et al* (1970) claim to be to a monoclinic phase although this has been disputed by Hidaka (1975). The fact that v^2 does not fall to zero for the relevant mode is consistent with the transition being first order. A determination of the value of $\bar{a}$ at which this transition to another phase would take place would require calculations of the lattice free energies in the two alternative structures.

6. Phase transitions in $KMnF_3$:Zn and $KZnF_3$:Mn

In §3 some static calculations for dilutely substituted crystals were presented; here we investigate possible dynamical roles of the impurities. In particular we attempt to

answer the questions: does the presence of Zn in $KMnF_3$ inhibit the rotations of F^- octahedra which cause the phase transition in the host, and does the presence of Mn in $KZnF_3$ induce these rotations? Our conclusions will necessarily be rather tentative.

In our investigations we have used a variety of computational techniques, including the program mentioned in §5.1 for finding equilibrium configurations of unit cells with lowered symmetry and the HADES code already mentioned in §3. We have also used 'supercell' methods to study collective instabilities, necessarily in a crystal in which the doping is highly concentrated and ordered on a superlattice. In the supercell method, which has been discussed by Sangster and Hussain (1985), mode frequencies and eigenvectors are found, by standard lattice dynamics techniques, for an enlarged periodic cell made up of repeated primitive cells of the host crystal with the substitution of a single centrally placed impurity. Relaxations around the impurity as well as an overall volume change determine the equilibrium configuration of the supercell. On enlarging the cell, the phonon branches of the primitive cell are folded back and some care has to be exercised in identifying the R_{25} mode. As well as considering the mapping on the resulting smaller Brillouin zone, the identification may be checked by treating a pure crystal supercell.

We have used the HADES code to look for local distortions around impurities in two configurations. Firstly we substituted an Mn^{2+} ion for Zn^{2+} in cubic $KZnF_3$ and introduced a rotation of the F^- octahedron surrounding the Mn^{2+} ion. (This procedure is similar to that adopted in studies of off-centre systems such as $KCl:Li^+$.) The F^- octahedron always relaxed back to the cubic configuration even when very high pressures were simulated by reductions in host lattice parameters. From this we conclude that if the host is constrained to be cubic at a distance from the impurity (i.e. on the boundaries of the explicitly treated region of around 200 atoms in the HADES calculations) then local rotations do not take place at all. Secondly we investigated a $KMnF_3$ host crystal in the tetragonal phase initially with a lattice parameter $\bar{a}$ only slightly below that required for the cubic to tetragonal transition and with a Zn^{2+} substitution. The local F^- octahedron showed some tendency to align with the axes defined by the neighbouring K^+ cuboid but there was no locally cubic region. On repeating this calculation with decreased $\bar{a}$, and therefore larger rotations of the F^- octahedron in the host, a similar tendency was found, that is around the Zn^{2+} impurity the rotation was partially quenched, and it could be seen that this quenching decreased rapidly with distance from the Zn^{2+} ion. One concern with this type of calculation is that constraints on the structure of the crystal remote from the impurity (the so-called region II of HADES calculations) may impose incorrect symmetries around the impurities. In these $KMnF_3$:Zn calculations such constraints would prevent the Zn^{2+} impurity 'seeding' a transition of the host to the cubic phase. As a further example, if a $KMnF_3$ crystal is constrained to be cubic at a lattice parameter well below that at which the transition takes place and a 'seeding' rotation of an F^- octahedron is introduced, relaxations again restore full cubic symmetry.

It was to allow for collective relaxations that we proceeded to supercell investigations. Due to computational limitations we were unable to treat supercells larger than $4 \times 4 \times 4$ primitive host cells. In all cases we made adjustments to the supercell volume to take account of the defect concentration; this is particularly important for the smaller cells. We examined the displacements of F^- ions in the eigenvectors for R_{25} vibrations in $KMnF_3$:Zn in the cubic phase. For small supercells we find that the displacements of F^- ions around the Zn^{2+} ions are smaller than those near the zone boundary. The effect is enhanced in larger supercells but, from our limited evidence, it

appears that even in dilutely doped systems there will always be some participation of the F^- ions which are immediate neighbours of Zn^{2+} in the mode. This is consistent with the above calculations of static relaxations in the tetragonal phase.

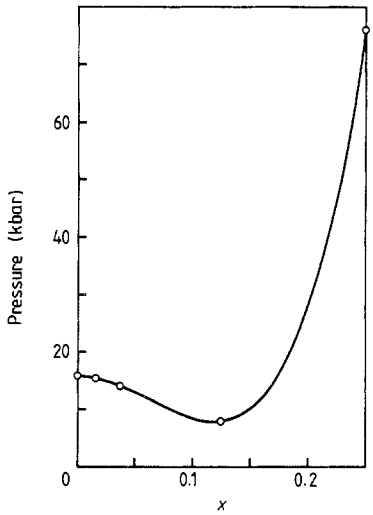

Figure 6. Transition pressures for $KMn_{1-x}Zn_xF_3$ ($0 \leq x \leq 0.25$).

We also found one rather surprising result from our supercell calculations for $KMn_{1-x}Zn_xF_3$ with $x \leq \frac{1}{4}$: If the supercell lattice parameter is reduced until the R_{25} frequency becomes imaginary and if this reduction in lattice parameter *from the appropriate equilibrium value* is interpreted as a transition pressure, using the compressibility for the composite crystal in each case, we obtain the curve shown in figure 6. The large increase in the transition pressure at the high end of the range is to be expected, since for $x = 1$ there is no transition, but the initial dip is unexpected. A possible interpretation of this effect is that the doping lowers the average interatomic separations and, since it is reductions in this distance which are eventually responsible for the pressure-induced phase transition, less pressure is required to achieve the transition. While the possibility cannot be ruled out that this effect is a spurious consequence of the artificial periodicity of defects, it should be noted that in the range of x for which the effect is found, the supercells are relatively large and there will be little interaction between defects.

Acknowledgments

Support for this work to all three authors from the Deutsche Forschungsgemeinschaft is gratefully acknowledged as is the funding of a three month visit to Regensburg University for MJLS from the DAAD (Deutscher Akademischer Austauschdienst).

References

Aleksandrov K S, Reshchikova L M and Beznosikov B V 1966 *Phys. Status Solidi* **18** K17
Barriuso M T and Moreno M 1984 *Phys. Rev.* B **29** 3623

Bilz H, Strauch D and Wehner R K 1984 *Handbuch der Physik* vol 25/2d, ed. S Flügge (Berlin: Springer)
Bruce A D and Cowley R A 1973 *J. Phys. C: Solid State Phys.* **6** 2422
Cao W and Barsch G R 1988 *Phys. Rev.* B **38** 7947
Catlow C R A, Diller K M and Norgett M J 1977a *J. Phys. C: Solid State Phys.* **10** 1395
Catlow C R A, Norgett M J and Ross T A 1977b *J. Phys. C: Solid State Phys.* **10** 1627
Cochran W and Cowley R A 1967 *Handbuch der Physik* vol 25/2a ed. S Flügge (Berlin: Springer) p 59
Cowley R A 1962 *Proc. R. Soc.* A **268** 121
—— 1964 *Phys. Rev.* **134** A981
Cox A and Sangster M J L 1985 *J. Phys. C: Solid State Phys.* **18** L1123
Dormann E, Copley J R D and Jaccarino V 1977 *J. Phys. C: Solid State Phys.* **10** 2767
Feder J and Pytte E 1970 *Phys. Rev.* B **1** 4803
Gesi K, Axe J D, Shirane G and Linz A 1972 *Phys. Rev.* B **5** 1933
Gesi K and Ozawa K 1973 *J. Phys. Soc. Japan* **34** 1698
Gesland J Y, Binois M and Nouet J 1972 *C. R. Acad. Sci., Paris* B **275** 551
Gillan M J 1981 *Phil. Mag.* A **43** 301
Hidaka M 1975 *J. Phys. Soc. Japan* **39** 180
Hirotsu S and Sawada S 1973 *Solid State Commun.* **12** 1003
Julliard J 1974 *Thèse 3e cycle* Université de Paris VI
Kilner J A 1981 *Phil. Mag.* A **43** 1473
Leblé A 1982 *Thèse d'Etat* Université du Maine
Lehner J N, Rauh H, Strobel K, Geick R, Heger G, Bouillot J, Renker B, Rousseau M and Stirling W G 1982 *J. Phys. C: Solid State Phys.* **15** 6545
Leibfried G and Ludwig W 1961 *Solid State Phys.* **12** 275
Norgett M J 1974 *AERE Harwell Report* R7650
—— 1977 *AERE Harwell Report* M288
Okazaki A and Suemune Y 1961 *J. Phys. Soc. Japan* **16** 671
Perry C H and Young E F 1967 *J. Appl. Phys.* **38** 4616
Ridou C, Rousseau M, Bouillot J and Vettier C 1984 *J. Phys. C: Solid State Phys.* **17** 1001
Rodríguez F and Moreno M 1986 *J. Phys. C: Solid State Phys.* **19** L 513
Rousseau M, Gesland J Y, Hennion B, Heger G and Renker B 1981 *Solid State Commun.* **38** 45
Sangster M J L and Atwood R M 1978 *J. Phys. C: Solid State Phys.* **11** 1541
Sangster M J L and Hussain A R Q 1985 *Physica* B **131** 119
Shirane G, Minkiewiwicz V J and Linz A 1970 *Solid State Commun.* **8** 1941
Vegard L 1921 *Z. Phys.* **5** 17